Journal of the Brazilian Society of Mechanical Sciences and Engineering manuscript No.
(will be inserted by the editor)

Numerical analysis of the influence of magnetic field waveforms on the performance of active magnetic regenerators

Fábio P. Fortkamp · Gusttav B. Lang · Jaime A. Lozano · Jader R. Barbosa Jr.

Abstract Keywords magnetic refrigeration · active magnetic regenerator · numerical modeling · magnetocaloric effect

1 Introduction

Mechanical vapor compression has been the dominant cooling technology for the past century [1] but, despite its dominance, it still faces an increasing number of challenges related to the its environmental footprint. The large entropy generation associated with vapor compression processes makes this techonology constrained by low exergy efficiencies, in particular for compact systems [2]. In addition, the phase-out of refrigerants with ozone depleting and global warming potentials has introduced the use of flammable substances, with their own set of risks for consumer applications [3] and technologial challenges [4].

The term *caloric cooling* is generally applied to alternative cooling techonologies in which the cooling effect is generated by the response of a solid material to a physical stimulus. The absence of hazardous gases, compressors and throttling devices makes these technologies potentially more efficient, scalable, silent and environmentally friendly. Magnetic refrigeration (MR) is the most advanced of all caloric technologies [2]; in particular, with the classes of magnetic refrigerants currently available, magnetocaloric refrigeration seems promising for applications in small temperature span (around 20 K), such as winecoolers and air conditioners [2].

In magnetic refrigeration, a *magnetocaloric material* (MCM) is subjected to a cyclical change of the applied magnetic field, and its temperature changes as a result of the *magnetocaloric effect* (MCE). The magnitude of the MCE depends on parameters related to characteristics of the material, magnetic field variation and temperature, and its maximal at the transition Curie temperature of the material. For a thorough introduction to the magnetocaloric effect and magnetocaloric materials, the reader is referred to [5].

Fábio P. Fortkamp
POLO — Research Laboratories for Emerging Technologies in Cooling and Thermophysics, Department of Mechanical Engineering, Federal University of Santa Catarina, Florianópolis, SC, 88040-900, Brazil, E-mail: fabio@polo.ufsc.br

Gusttav B. Lang · Jaime A. Lozano · Jader R. Barbosa Jr.
POLO — Research Laboratories for Emerging Technologies in Cooling and Thermophysics, Department of Mechanical Engineering, Federal University of Santa Catarina, Florianópolis, SC, 88040-900, Brazil

For operating conditions typical of a low-temperature span magnetic refrigerator, the MCE is typically on the order of 2-5 K. To amplify this temperature change, heat regeneration is usually employed [6]. Active magnetic regenerators (AMR) are thermal devices where the magnetocaloric material constitutes a solid matrix through which flows an aqueous heat transfer fluid, and is cyclically magnetized and demagnetized to activate the magnetocaloric effect. A regenerator is essentially a cascade of infinitesimal "layers" of MCM that are activated simultaneously to build up a temperature profile along its length. These layers can be made of the same material, yielding an homogeneous regenerator; however, given the dependence of the MCE with temperature, it is an interesting strategy to build *multilayer* regenerators, where each layer is composed of a different material that will work around its own Curie temperature, maximizing the magnetocaloric effect of each portion.

The five main subsystems in an AMR-based magnetic refrigerator can be identified as follows [7,8]:

1. magnetic circuit;
2. active magnetic regenerator;
3. flow management system;
4. control system;
5. transmission system;
6. heat exchangers and cabinet.

The magnetic circuit generates oscillating magnetic fields that activate the MCE in the active magnetic regenerators. As previously explained, the regenerators are composed of magnetocaloric porous media, and the flow management system provides the alternating fluid flow through the beds. The control system serves the purpose of synchronizing the fluid flow regime with the magnetic field variations. Finally, the heat exchangers are responsible for transferring the cooling effect from the AMR to the refrigerated cabinet and the rejected heat to the surroundings.

Magnetic refrigerators can operate according to different thermodynamic cycles, but the stages are roughly as follows. The magnetic circuit magnetizes the MCM, increasing its temperature due to the MCE. During the so-called *cold blow*, cold fluid from the cold source flows through the warm bed and absorbs its energy, releasing it to the external heat exchanger. On the return of the fluid, the solid is demagnetized and cooled down, and in the *hot blow* the fluid relases energy to the bed, decreasing its temperature so it can absorb the thermal load at the cold source. The cycle then repeats; different cycles can be configured by different durations and synchronization steps between these two *characteristic waveforms*:

1. The *magnetic profile*, which describes the oscillating magnetic field over one regenerator;
2. The *fluid flow profile*, which describes the time-variation of flow rate through one bed.

Among the challenges cited in the literature for further improvement of magnetic refrigerators, two can be highlighted [9]:

1. Better use of AMR and magnetic circuit models during the design process, to identify optimal geometric and operating parameter;
2. Better study of losses that are present in a magnetic cooling device.

In other words, these challenges arise due to *interactions* between different subsystems of a magnetic refrigerator. In these context, the focus on the aforementioned waveforms is a suitable approach for optimizing the performance of magnetic refrigerators, as these profiles represent interactions between systems. As it will be seen, mathematical models for AMRs take these waveforms as input, and they are generated by models for other components.

Fluid flow profiles are more easily investigated with experimental methods, since they can be altered with modifications in the fluid flow system. In particular, the *duration* of blows have been extensively investigated [10, 11, 12], and the literature shows that the cooling capacity of magnetic refrigerators can be increased by focusing fluid flows during periods where the magnetic field is at its extrema values.

In this work, we focus on magnetic profiles, which are less studied in the literature. The studied waveforms are depicted in Figure 1, identified by the transitions between states. The instantaneous profile represents step-like changes between high and low levels of the magnetic field, while the ramp profile has linear variations between these states. The rectified cosine profile is a common waveform found in the literature that has a continuous variation of the applied magnetic field.

profiles_all-eps-converted-to.pdf

Fig. 1: Magnetic profiles studied in this paper

The instantaneous magnetic profile is characteristic of the Brayton AMR cycle, where the magnetization and demagnetization steps must be done adiabatically, as shown in Figure 2; compared to other common cycles such as the Ericsson, the Brayton cycle results in the highest cooling capacities for the same operating parameters [6], at the expense of lower coefficient of performance.

Fig. 2: Brayton AMR cycle

In practice, the ramp profile is a more feasible realization with finite transition times, and its synchronization with the fluid flow profile can yield different performance levels [13]. In particular, the plateaus of magnetic field should be centered with the blow durations [14]. Figure 3 shows the syncronization schema between the magnetic and fluid flow profiles, showing the ramp magnetic profile as an example.

This paper uses the AMR model developed by [15], and the same authors had studied magnetic profiles waveforms in an earlier work [16]. However, their amplitudes was not varied, nor were they investigated with different geometries.

The present works combines the gaps from the above cited papers in investigating the performance of a magnetic refrigerator under different magnetic profile waveforms. These profiles_rm_and_flow_instantaneous-eps-converted-to.pdf

Fig. 3: Ramp magnetic profile (solid lines) and instantaneous fluid flow profile (dashed lines)

waveforms are mathematically modeled, and the cooling capacity and coefficient of performance are calculated based on the profiles parameters, while also investigated how the AMR geometry affect the performance in combinations with the magnetic profile. The fluid flow profile is assumed fixed in shape, although its parameters are also variied. The emulate constraints on an operating point of actual magnetic refrigeration devices, the temperature span is set fixed, and hence few comments are made on second-law efficiency.

2 Materials and methods

In this work, we perform numerical simulations of a previously developed AMR model, varying the profile and geometric parameters. We also couple a model for calculating the power comsumption of a proposed valve system, a topic understudied in the literature. With this, we can evaluate the influence of the profile on cooling capacity and coefficient of performance.

2.1 AMR model

2.1.1 Governing equations

Simulations were performed using a one-dimensional AMR mathematical model [16,15]. Here we will show a summarized version focusing on the governing equations. This model solves momentum and energy balance equations for the solid and fluid phases, represented by indices 's' and 'f', respectively. The model geometry is depicted in Figure 4, and assumes regenerators composed of monodisperse packed spheres with porosity ε.

The momentum equation for the fluid domain is:

$$\frac{\rho_{\mathrm{f}}}{\varepsilon}\frac{\partial V_z}{\partial t} = -\frac{\partial P}{\partial z} - \frac{\mu_{\mathrm{f}}}{K}V_z - \frac{c_{\mathrm{E}}\rho_{\mathrm{f}}}{K^{1/2}}\left|V_z\right|V_z \tag{1}$$

and is solved for the time-dependent uniform fluid velocity through the bed.

The energy equation for the fluid phase can be written as:

reg3d-eps-converted-to.pdf

Fig. 4: AMR model geometry

$$\begin{aligned}\rho_{\mathrm{f}} c_{p,\mathrm{f}} \left(\varepsilon \frac{\partial T_{\mathrm{f}}}{\partial t} + V_z \frac{\partial T_{\mathrm{f}}}{\partial z} \right) = & - \hbar_{\mathrm{sf}} \beta \left(T_{\mathrm{f}} - T_{\mathrm{s}} \right) \\ & + \left| V_z \left. \frac{\partial p}{\partial z} \right|_f \right| \\ & + \varepsilon \left(k_{\mathrm{f}}^{\mathrm{eff}} + \rho_{\mathrm{f}} c_{p,\mathrm{f}} D_{\mathrm{ld}} \right) \frac{\partial^2 T_{\mathrm{f}}}{\partial z^2} \\ & + \dot{q}_{\mathrm{csg}}\end{aligned} \tag{2}$$

while the energy equation for the solid phase is written as:

$$\rho_{\mathrm{s}} c_{\mathrm{s}} (1-\varepsilon) \frac{\partial T_{\mathrm{s}}}{\partial t} = \hbar_{\mathrm{sf}} \beta (T_{\mathrm{f}} - T_{\mathrm{s}}) + (1-\varepsilon) k_{\mathrm{s}}^{\mathrm{eff}} \frac{\partial^2 T_{\mathrm{s}}}{\partial z^2} \tag{3}$$

Initial and boundary conditions, solution methods, convergence analyses, and closure relations for the porous media terms are described in [15]. This AMR model solves the above equations for one regenerator operating between given sources temperatures, during one full cycle (hot and cold blows and magnetization and demagnetization periods), given specified operating conditions (to be discussed later).

The casing heat transfer term $\dot{q}_{\mathrm{csg}}$ in Equation 2 is calculated solving the heat conduction in the regenerators casing [15], and can be neglected to simplify some analyses. More details are provided in section 3.

2.1.2 How the fluid flow profile is used

The pressure gradient in Equation 1is modeled as:

$$-\frac{\partial P}{\partial z} = \rho_{\mathrm{f}} A_{\mathrm{t}} g(t) \tag{4}$$

where $g(t)$ is a dimensionless function that expresses the mathematical waveform of the pressure gradient, and A_{t} is its amplitude, adjusted in a convergence loop; the mass flow rate calculated from the Darcy velocity from Equation 1 is compared with the input value of mass flow rate until these values converge. The waveform $g(t)$ represents the fluid flow profile used.

2.1.3 How the magnetic profile is used

The magnetic profile is modeled by a waveform of magnetic field strength H applied perpendicular to the regenerators, as shown in Figure 4. The magnetic field is assumed uniform throughout the beds. The applied field is corrected from demagnetization effects to yield the effective field inside the regenerators:

$$H^{\text{eff}} = H - N_{\text{D}} M \tag{5}$$

where M is the magnetization field of the material, and N_{D} is a demagnetization factor.

The magnetocaloric effect is implemented in the so-called discrete approach [17]; every time the magnetic field changes, based on the input magnetic profile, the solid temperature is calculated according to:

$$T_{\text{s}}(t + \Delta t) = T_{\text{s}}(t) + \Delta T_{\text{ad}} \left(T_{\text{s}}(t), H^{\text{eff}}(t), H^{\text{eff}}(t + \Delta t) \right) \tag{6}$$

where the adiabatic temperature variation ΔT_{ad} is calculated from tabulated experimental data for magnetocaloric materials as function of temperature and effective field. [15].

2.1.4 Evaluation of solid and fluid properties

The fluid properties are considered constant in the momentum equation to decouple the solution procedures to determine the velocity and temperature fields. The properties are computed at the average temperature between the hot and cold sources temperatures, and are evaluated from interpolated tables exported from the EES software [18]. In all simulations shown in this work, the heat transfer fluid is a mixture of water/ethylene-glycol with concentration 80/20 % vol. For the energy equations, the fluid properties are also calculated from tabulated data, but the temperature dependence is considered.

n this chapter, all simulations use gadolinium or its allows as the magnetocaloric material. Gadolinium is a benchmark material with a Curie temperature of 290 K. For simplicity, the solid density is assumed constant at $\rho_{\text{s}} = 7900\,\text{kg/m}^3$ and the solid thermal conductivity is set to $k_{\text{s}} = 10.5\,\text{W}/(\text{m}\,\text{K})$. The specific heat capacity of Gd is calculated as a function of temperature and magnetic field based on experimental data, using a bi-linear interpolation scheme; more details on the experimental dataset are available in [15].

In this work, both single- and multilayer regenerators are considered. For the multilayer simulations, alloys of gadolinium and yttrium are used in the form $\text{Gd}_{1-x}\text{Y}_x$, where x is the yttrium fraction. This fraction decreases the Curie temperature of the alloy relative to that of pure gadolinium. Due to the lack of experimental data on the magnetocaloric properties of $\text{Gd}_{1-x}\text{Y}_x$ alloys at the time this analysis was made, a simpler approach was used in which the properties of alloys with a low yttrium fraction are identical to those of pure gadolinium, except for the Curie temperature (which is shifted to lower values).

2.1.5 Performance metrics

The AMR model considers only one bed and assumes N_r identical beds experience the same cycle, multiplyind the performance metrics below by this factor

number of regenerators

The cooling capacity is calculated as [15]:

$$\dot{Q}_\mathrm{C} = N_\mathrm{r}\frac{1}{\tau}\int_{\tau_\mathrm{HB}} \dot{m}_\mathrm{f}(t)c_{p,\mathrm{f}}\left(T_\mathrm{C} - T_\mathrm{f,CE}\right)\mathrm{d}t \tag{7}$$

where τ is the cycle period, and τ_HB is the duration of the hot blow, during which the cold end temperature is compared to the cold source temperature.

The magnetic power to operate the AMR cycle is modeled as the ideal Carnot power, ignoring most thermal irreversibilities:

$$\dot{W}_\mathrm{mag} = \dot{Q}_\mathrm{C}\frac{T_\mathrm{H} - T_\mathrm{C}}{T_\mathrm{C}} \tag{8}$$

while the fluid friction irreversibility is accounted for in the calculation of the pumping power:

$$\dot{W}_\mathrm{pump} = N_\mathrm{r}\frac{1}{\tau}\int_0^\tau \frac{\dot{m}_\mathrm{f}}{\rho_\mathrm{f}}\Delta P\,\mathrm{d}t \tag{9}$$

where ΔP is the total pressure drop through the regenerator.

2.2 Hydraulic system and fluid flow profile model

The canonical fluid flow profile considered in this work is the square wave or *instantaneous profile*, because of the instantaneous change in flow rate, as shown in Figure 5.

The instantaneous mass flow rate, $\dot{m}_\mathrm{f}(t)$, is defined over a cycle with a period τ, and represents the fluid flow through a given regenerator bed. The so-called *hot cycle*, during which the MCM is magnetized, occupies the time interval $0 \le t < \tau/2$, while the *cold cycle* lies between $\tau/2 \le t \le \tau$. The flow profile oscillates between two plateaus of equal magnitude $\dot{m}_\mathrm{f,max}$ and opposite directions, which are centered in each half-cycle. During the hot cycle, the cold blow period is τ_CB, and during the cold cycle the hot blow period is τ_HB. If the flow is balanced, then $\tau_\mathrm{CB} = \tau_\mathrm{HB}$.

During each half cycle, there are periods without fluid flow, defined as:

$$\tau_\mathrm{0,HC} = \frac{\tau/2 - \tau_\mathrm{CB}}{2} \tag{10}$$

$$\tau_\mathrm{0,CC} = \frac{\tau/2 - \tau_\mathrm{HB}}{2} \tag{11}$$

where HC and CC stand for hot cycle and cold cycle, respectively.

The profile can be mathematically defined as:

$$\dot{m}_\mathrm{f}(t) = \begin{cases} 0, & 0 \le t < \tau_\mathrm{0,HC} \\ \dot{m}_\mathrm{f,max}, & \tau_\mathrm{0,HC} \le t \le \tau/2 - \tau_\mathrm{0,HC} \\ 0, & \tau/2 - \tau_\mathrm{0,HC} < t < \tau/2 + \tau_\mathrm{0,CC} \\ -\dot{m}_\mathrm{f,max}, & \tau/2 + \tau_\mathrm{0,CC} \le t \le \tau - \tau_\mathrm{0,CC} \\ 0, & \tau - \tau_\mathrm{0,CC} < t < \tau \end{cases} \tag{12}$$

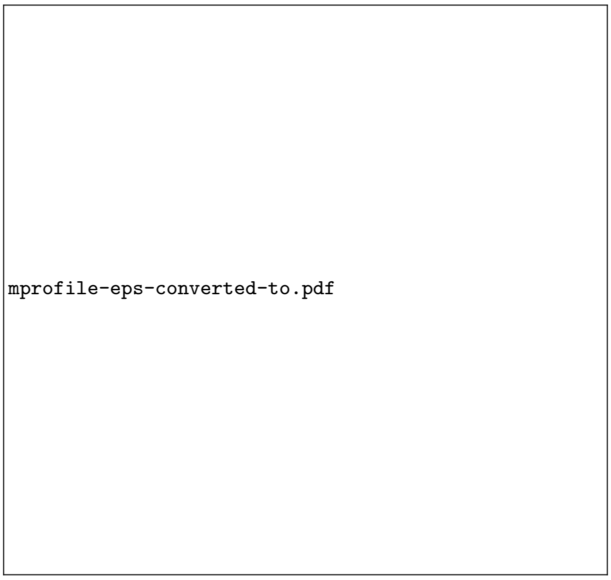

Fig. 5: Instantaneous fluid flow profile

When the blows have different time durations, the AMR cycle is considered unbalanced, and this is known to have a negative effect on performance [19, 11]. In this work, the blows are always balanced, hence the blow fraction, the ratio of blow durations to cycle period [11], can be evaluated as:

$$F_{\mathrm{B}} = \frac{2\tau_{\mathrm{B}}}{\tau} \tag{13}$$

where τ_{B} is the duration of one blow.

The hydraulic system to modulate this fluid flow through different regenerators at different time instants is composed of a pump and a set of electronic valves which can be precisely controlled to yield the desired blow durations. The electrical power consumed by the valve array is computed separately from other work contributions. An application of electronic valves in AMR devices has been presented by [20].

Due to evolving developments in our group, two types of valves are considered, as will be elaborated in section 3.

The first approach, called *Type B valves*, uses the model of [21], assuming that the individual consumption of each valve is independent of frequency and blow fraction. The valve power $\dot{W}_{\mathrm{valve}}$ can be computed as:

$$\dot{W}_{\mathrm{valve}} = N_{\mathrm{v}} F_{\mathrm{B}} \left(\dot{W}_{\mathrm{valve,n}} + \frac{1}{2} \dot{W}_{\mathrm{relay,n}} \right) \tag{14}$$

where N_{v} is the number of valves, $\dot{W}_{\mathrm{valve,n}}$ is the measured average nominal power for one normally-closed electronic valve and $\dot{W}_{\mathrm{relay,n}}$ is the nominal power for one controlling relay. The factor $1/2$ is due to two valves being controlled by one relay.

In the second approach, *Type A* valves are used, with lower nominal power but that depends on frequency and blow fraction. For these valves, the valve power was experimentally correlated as:

$$\dot{W}_{\mathrm{valve}}\,[\mathrm{W}] = N_{\mathrm{v}}\left(0.927f\,[\mathrm{Hz}] + 1.023F_{\mathrm{B}} + 0.226f\,[\mathrm{Hz}]F_{\mathrm{B}} - 0.037\right) \tag{15}$$

Equation (15) was correlated for blow fractions of 50 and 100 % and for frequencies in the range of 0.2–1.6 Hz, with an uncertainty on the order of 0.4 W for a single valve. The use of different valve types will be discussed among the presented results.

Indepedent of the valve type used, it is also assumed that this valve system can produce the fluid flow profile shown in Figure 5, where the displaced fluid mass during one blow in one regenerator bed is $\dot{m}_{\mathrm{f,max}} F_{\mathrm{B}}\, \tau/2$.

The *utilization factor* can then be calculated as:

$$\Phi = \frac{\dot{m}_{\mathrm{f,max}} F_{\mathrm{B}} c_{\mathrm{s}}}{2 f m_{\mathrm{s}} c_{\mathrm{s}}} \tag{16}$$

For an even number of poles in the magnetic circuit, it may be advantageous to employ an odd number of regenerator beds to break the symmetry between the magnetic circuit and the beds, thus avoiding positions of equilibrium between magnetic forces which result in torque oscillations [22]. Additionally, in general, two valves per regenerator may be necessary (one at each end), to independently control the hot and cold blows for each bed and correct flow imbalance; thus, in all results in this work, the number of valves is calculated as:

$$N_{\mathrm{v}} = 2N_{\mathrm{r}} \tag{17}$$

2.3 Calculation of the coefficient of performance

The coefficient of performance takes the cooling capacity as the main output parameter from the AMR model, in addition to all previously cited power contributions:

$$\mathrm{COP} = \frac{\dot{Q}_{\mathrm{C}}}{\dot{W}_{\mathrm{pump}} + \dot{W}_{\mathrm{mag}} + \dot{W}_{\mathrm{valve}}} \tag{18}$$

2.4 Definition of magnetic profiles

The magnetic profiles considered in this work were shown in Figure 1; here their mathematical definitions are presented. The profiles are presented in terms of the flux density $B = \mu_0 H$, where μ_0 is the permeability of free space; the magnetic field H is used in the evaluation of the magnetocaloric effect (cf. subsubsection 2.1.3).

The instantaneous profile (represented by the subscript "IT") and the rectified cosine profile (represented by "RC") are defined solely in terms of the (extreme) values B_{min} and B_{min}:

$$B_{\mathrm{IT}}(t) = \begin{cases} B_{\mathrm{max}}, & 0 \le t < \tau/2 \\ B_{\mathrm{min}}, & \tau/2 \le t < \tau \end{cases} \tag{19}$$

$$B_{\mathrm{RC}}(t) = B_{\mathrm{min}} + \left(B_{\mathrm{max}} - B_{\mathrm{min}}\right)\left|\cos\left(\frac{\pi}{\tau}\left(t - \frac{\tau}{4}\right)\right)\right| \tag{20}$$

As previously discussed, a suitable approximation of the instantaneous profile is the *magnetic ramp profile*, shown in Figure 6. The so-called *hot cycle*, during which the MCM is magnetized, occupies the range $0 \leq t < \tau/2$, while the *cold cycle* lies in the range $\tau/2 \leq t < \tau$. The magnetic profile oscillates between a low value B_{min} and a high value B_{max}, and remains at each plateau for a period of τ_{M}. The plateaus are balanced and centered at each half-cycle.

Fig. 6: Magnetic ramp profile

The *ramp period* τ_{R} is defined as:

$$\tau_{\mathrm{R}} = \frac{1}{4}\left(\tau - 2\tau_{\mathrm{M}}\right) \tag{21}$$

such that there are four ramp periods in one full cycle. The ramp rate, θ_{R}, is:

$$\tan\theta_{\mathrm{R}} = \frac{\left(B_{\mathrm{max}} - B_{\mathrm{min}}\right)}{2\tau_{\mathrm{R}}} \tag{22}$$

The magnetization fraction, F_{M}, is the fraction of the cycle during which the magnetocaloric material is subjected to a constant magnetic field:

$$F_{\mathrm{M}} = \frac{2\tau_{\mathrm{M}}}{\tau} \tag{23}$$

The ramp profile (“RM”) can be mathematically defined as:

$$B_{\mathrm{RM}}(t) = \begin{cases} (B_{\mathrm{max}}+B_{\mathrm{min}})/2 + t\tan\theta_{\mathrm{R}}, & 0 \leq t < \tau_{\mathrm{R}} \\ B_{\mathrm{max}}, & \tau_{\mathrm{R}} \leq t < \tau/2 - \tau_{\mathrm{R}} \\ B_{\mathrm{max}} - \left(t - \left(\tau/2 - \tau_{\mathrm{R}}\right)\right)\tan\theta_{\mathrm{R}}, & \tau/2 - \tau_{\mathrm{R}} \leq t < \tau/2 + \tau_{\mathrm{R}} \\ B_{\mathrm{min}}, & \tau/2 + \tau_{\mathrm{R}} \leq t < \tau - \tau_{\mathrm{R}} \\ B_{\mathrm{min}} + \left(t - \left(\tau - \tau_{\mathrm{R}}\right)\right)\tan\theta_{\mathrm{R}}, & \tau - \tau_{\mathrm{R}} \leq t \leq \tau \end{cases} \tag{24}$$

Additionally, the average values of the magnetic field during each half-AMR cycle are considered for comparison between profiles. The average magnetic profile during the hot cycle ($0 \leq t < \tau/2$) is denoted $\overline{B}_{\mathrm{high}}$ and the average during the cold cycle ($\tau/2 \leq t < \tau$) is denoted $\overline{B}_{\mathrm{low}}$. For the instantaneous waveform, these average values are identical to the extrema values.

3 Results and Discussions

The analysis of magnetic profiles was performed in two different stages in the research of our group, as discussed below.

3.1 Comparison of instantaneous and rectified cosine profiles using a simplified model

In the first stage, the instantaneous and rectified cosine profiles are compared in the AMR model, considering monolayer regenerators without casing losses, and using Type B valves. The parameters used in all simulations are presented in Table 1.

Table 1: AMR parameters kept fixed in the simulations with different magnetic profiles

Parameter	Value
D_p	0.5 mm
H_r	20 mm
W_r	25 mm
L_r	100 mm
N_r	11
N_v	22
T_H	298 K
T_C	278 K
$\dot{W}_{NV}$	4 W
$\dot{W}_R$	0.36 W

When comparing the performances resulting from the application of the different magnetic profiles, the average magnetic field during the hot cycle will be considered the same; this implies a higher peak for the rectified cosine. For the cold cycle, two comparison methods are considered, as shown in Figure 7:

1. The minimum values for both profiles is the same;
2. The average value for both profiles during the cold cycle is the same.

For reference, in all simulations, the minimum value for the rectified cosine was fixed at $B_{\mathrm{min,RC}} = 0.1\,\mathrm{T}$. In the first comparison, the minimum value for the instantaneous waveform was kept at the same level ($B_{\mathrm{min,IT}} = B_{\mathrm{min,RC}}$); hence, the average low value for the RC profile was higher ($\overline{B}_{\mathrm{low,RC}} > \overline{B}_{\mathrm{low,IT}}$). This represents common design scenarios: a constant low-valued plateau for the magnetic field for instantaneous-like magnetic profiles [23,24], or a low peak for the rectified cosine profile [25]. For the other comparison method, the low level of the instantaneous profile was increased ($B_{\mathrm{min,IT}} > B_{\mathrm{min,RC}}$) in order to keep the same average ($\overline{B}_{\mathrm{low,RC}} = \overline{B}_{\mathrm{low,IT}}$).

In addition, simulations were carried out for various values of blow fraction; the rectified cosine profile can benefit from a smaller blow fraction because this can concentrate the flow during the periods of very high or low fields. In this section, all results use the critical value of blow fraction that maximized the cooling capacity: fluid flowing during the entire period for the instantaneous profile, and only during 60 % of the period (the smallest blow fraction tested) for the cosine profile; this latter case is shown in Figure 8.

Figure 9 shows the cooling capacity attained by the device at a frequency of 1 Hz and different utilizations, for both comparison methods. The horizontal axis shows the average

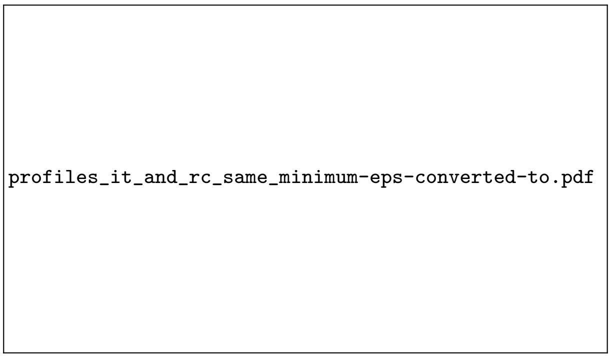

(a) Same minimum

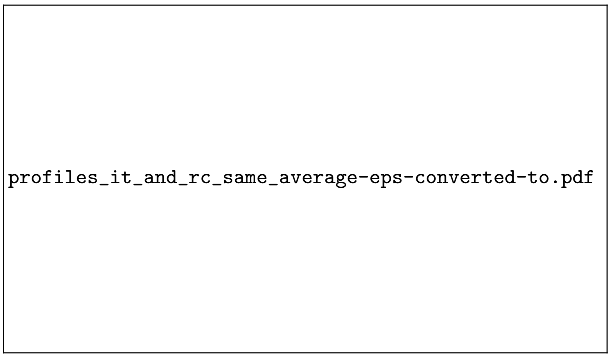

(b) Same average

Fig. 7: Comparison methods for the instantaneous and rectified cosine profiles

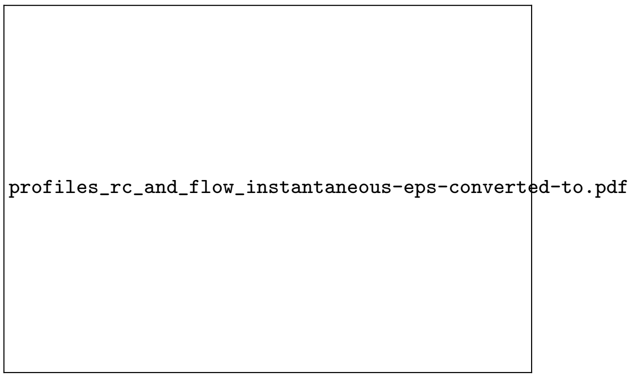

Fig. 8: Rectified cosine magnetic profile and the instantaneous flow profile with blow fraction of 60 %

value during the high field region. For Fig. 9a, the instantaneous profile almost always yields a higher performance, while for Fig. **??** the rectified cosine profile generates higher cooling capacities. Since the average field during the hot cycle (high field stage) is the same, the main difference is due to the low magnetic field levels. For the "same minimum" comparison, the instantaneous profile is capable of keeping the magnetic field at low levels for the whole half-cycle, which is beneficial for performance; for $\Phi = 1.0$ and $\overline{B}_{\mathrm{high}} = 1.40\,\mathrm{T}$, the cooling capacity for the instantaneous profile is 196.3 % higher than for the cosine profile. As demonstrated by [16], a higher average magnetic field during the low-field stage increases the solid temperature and consequently results in warmer fluid entering the cold heat exchanger, representing a thermal loss. In the "same-average" comparison, the cosine profile is capable of achieving much lower levels (since its minimum value is fixed), therefore providing more cooling power. However, as explained before, this analysis serves mainly the purpose of illustrating the influence of low magnetic field variation, by looking at two hypothetical scenarios. More complex magnetic circuit geometries are required to generate the instantaneous magnetic profile with a low magnetic field close to 0.

Qc_B_comp_f_1_same_minimum-eps-converted-to.pdf

(a) Same minimum

Fig. 9: Cooling capacity as a function of the average high magnetic field, for different utilizations. "IT": instantaneous (blow fraction of 100 %); "RC": rectified cosine (blow fraction of 60 %), for both comparison methods.

The only exception in the "same minimum" comparison is seen for the lowest utilization of $\Phi = 0.2$, where the performance is slightly better for the RC profile. Since the blow fraction for the cosine is lower, the mass flow rate is higher in the latter for the same utilization (cf. Eq. (20)). This increases the heat transfer rate, as previously explained — outweighing the effects of the magnetic field.

The same analysis, but in terms of the coeficient of performance, is shown in Figure 10. For the "same average" analysis, the COP results show the same trends as the cooling capacity. However, for the somewhat more realistic analysis where the minimum of both profiles are the same, the rectified cosine profile yields better results for small values of utilization. This is due to a lower pumping power, as the mass flow rate for the cosine profile is slightly higher, but also flows for a shorter period of time. Since in this region the cooling capacity for the RC profile can be close to or higher than the IT profile (cf. Fig. 9a), the coefficient of performance becomes higher for the rectified cosine profile.

COP_B_comp_f_1_same_minimum-eps-converted-to.pdf

(a) Same minimum

Fig. 10: Coefficient of performance as a function of the average high magnetic field, for different utilizations. “IT”: instantaneous (blow fraction of 100 %); “RC”: rectified cosine (blow fraction of 60 %), for both comparison methods.

In general, considering the goal of achieving target requirements for the cooling capacity, AMRs operating with the instantaneous magnetic profile generate better performance results. As can be seen in Fig. 9, an instantaneous profile with the lowest possible value of B_{min} and the highest possible value of B_{max}, with a flow profile occupying the whole cycle with average values of utilization, results in the highest values of cooling capacity among all simulations.

The rectified cosine profile, found in compact systems using Halbach arrays, can surely benefit from reducing the blow fraction, both in terms of cooling capacity and temperature span. However, for the typical parameters evaluated in this Thesis, even if the blow fraction is optimized for the “RC” profile, the “IT” profile still yields better results.

3.1.1 Analysis of the instantaneous profile

As shown in the previous section, the instantaneous profile generally yields the highest values of cooling capacity. Therefore, in this section, a more detailed analysis of this profile has been carried out, where the maximum field in **??** is varied, while the minimum value is kept at 0.05 T. Figure 11 shows the cooling capacity as a function of the utilization, for several levels of the maximum magnetic field and two different operating frequencies. Because of the conflict between a low heat transfer rate for flow rates that are too low and losses in regenerator effectiveness in flow rates that are too high, there are critical values of utilization that maximize the cooling capacity, and this critical values increases with the magnetic field. For higher magnetic fields, the increase in the MCE surpasses the loss of effectiveness, and one can go to higher flow rates without losing performance. It can also be seen in Fig. 11 that at higher frequencies the values of cooling power are higher, and also the critical values of utilization are lower; however, this is usually achieved at the expense of a higher power consumption in AMR devices at higher frequencies [26, 27].

The parameters in Table 1 were chosen from preliminary simulations, so they are not optimal. To understand the impact of the regenerator geometry on the performance with the instantaneous profile, the regenerator height was varied in Fig. 12, and all other parameters

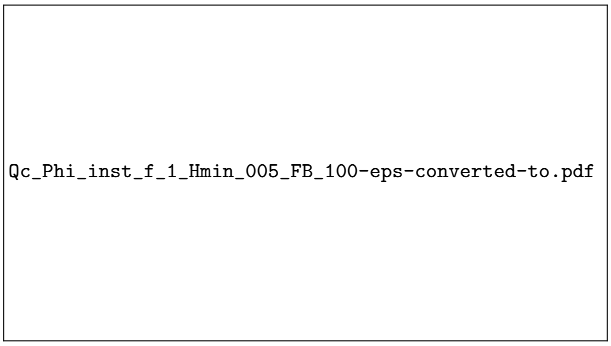

(a) $f = 1\,\mathrm{Hz}$

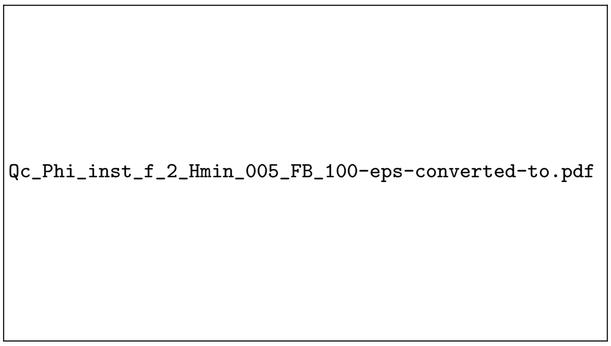

(b) $f = 2\,\mathrm{Hz}$

Fig. 11: Cooling capacity as a function of utilization, for various values of the high magnetic field for the instantaneous profile

from Table 1 were kept fixed and with $\phi = 0.4$. As expected, higher magnetic fields allow for smaller regenerators (hence more compact systems) to achieve a desired cooling capacity. For instance, to achieve a capacity of 100 W, increasing the field from 1.0 to 1.2 T results in regenerators that are 36 % smaller. Comparing results for cooling capacity and coefficient of performance, the trends are largely the same, as the former is more sensitive to variations in the magnetic field and regenerator height than the components of power.

Acknowledgements This work was supported by CNPq, Embraco and EMBRAPII Unit Polo/UFSC.

References

1. P. Bansal, E. Vineyard, O. Abdelaziz, International Journal of Sustainable Built Environment **1**, 85 (2012)
2. A. Kitanovski, U. Plaznik, U. Tomc, A. Poredoš, International Journal of Refrigeration **57**(Supplement C), 288 (2015). DOI https://doi.org/10.1016/j.ijrefrig.2015.06.008
3. IIR. 36th informatory note on refrigeration technologies: Flammable refrigerants. Available at `http://www.iifiir.org/userfiles/file/publications/notes/NoteTech_36_EN_nkyix2fcj7.pdf` (2017). Accessed on October 30th, 2018
4. S. Lionte, M. Risser, C. Vasile, L. Elouad, C. Muller, International Journal of Refrigeration **85**, 303 (2018). DOI 10.1016/j.ijrefrig.2017.10.009

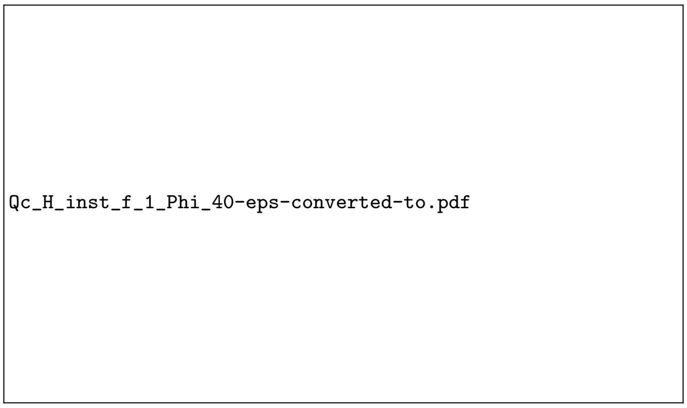

(a) Cooling capacity

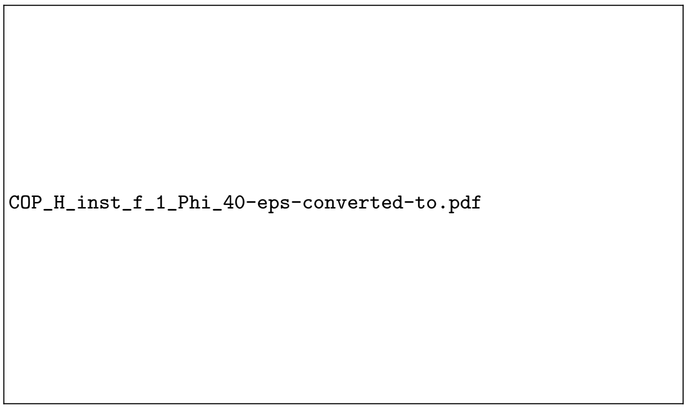

(b) Coefficient of performance

Fig. 12: Performance metrics as a function of the regenerator height (all other parameters were set as in Table 1, for utilization factor of 0.4) for various values of the high magnetic field of the instantaneous profile

5. A. Smith, C.R.H. Bahl, R. Bjørk, K. Engelbrecht, K.K. Nielsen, N. Pryds, Advanced Energy Materials **2**, 1288 (2012)
6. A. Kitanovski, U. Plaznik, J. Tušek, A. Poredoš, International Journal of Refrigeration **37**, 28 (2014)
7. J.A. Lozano, Cadena, Designing a rotary magnetic refrigerator. Mechanical Engineering, Federal University of Santa Catarina, Florianópolis (2015)
8. P.V. Trevizoli, T.V. Christiaanse, P. Govindappa, I. Niknia, R. Teyber, J.R. Barbosa, Jr., A. Rowe, Science and Technology for the Built Environment **22**(5), 507 (2016). DOI 10.1080/23744731.2016.1171632
9. D. Eriksen, Active magnetic regenerator refrigeration with rotary multi-bed technology. Department of Energy Conversion and Storage, Technical University of Denmark, Denmark (2016)
10. R. Teyber, P.V. Trevizoli, I. Niknia, T.V. Christiaanse, P. Govindappa, A. Rowe, International Journal of Refrigeration **74**, 38 (2017)
11. A.T.D. Nakashima, S.L. Dutra, P.V. Trevizoli, J.R. Barbosa, Jr., International Journal of Refrigeration **93**, 236 (2018)
12. F.P. Fortkamp, D. Eriksen, K. Engelbrecht, C.R.H. Bahl, J.A. Lozano, J.R. Barbosa, Jr., International Journal of Refrigeration **91**, 46 (2018). DOI 10.1016/j.ijrefrig.2018.04.019
13. J. Tušek, A. Kitanovski, I. Prebil, A. Poredoš, International Journal of Refrigeration **34**(6), 1507 (2011). DOI 10.1016/j.ijrefrig.2011.04.007

14. R. Bjørk, K. Engelbrecht, International Journal of Refrigeration **34**, 192 (2011). DOI 10.1016/j.ijrefrig.2010.07.004
15. P.V. Trevizoli, A.T. Nakashima, J.R. Barbosa, Jr., International Journal of Refrigeration **72**(206-217) (2016)
16. P.V. Trevizoli, J.R. Barbosa, Jr., A. Tura, D. Arnold, A. Rowe, Journal of Thermal Science and Engineering Applications **6** (2014)
17. K.K. Nielsen, J. Tusek, K. Engelbrecht, S. Schopfer, A. Kitanovski, C.R.H. Bahl, A. Smith, N. Pryds, A. Poredos, International Journal of Refrigeration **34**, 603 (2011)
18. S.A. Klein. EES — Engineering Equation Solver, Professional Version v9.339. F-Chart Software (2013). Available at `http://fchart.com`.
19. D. Eriksen, K. Engelbrecht, C.R.H. Bahl, R. Bjørk, K.K. Nielsen, Applied Thermal Engineering **103**, 1 (2016)
20. A.T.D. Nakashima, S.L. Dutra, G. Hoffmann, J.A. Lozano, J.R. Barbosa, Jr., in *Proceedings of the 8th International Conference on Caloric Cooling (Thermag VIII)* (Darmstadt, Germany, 2018)
21. P.O. Cardoso, M.C. Destro, M.G. Alvarez, J.A. Lozano, J.R. Barbosa, Jr., V.J. de Negri, in *Proceedings of the 16th Brazilian Congress of Thermal Sciences and Engineering* (Vitória, 2016)
22. D. Eriksen, K. Engelbrecht, C.R.H. Bahl, R. Bjørk, K.K. Nielsen, A.R. Insinga, N. Pryds, International Journal of Refrigeration **58**, 14 (2015)
23. A.R. Insinga, Optimising magnetostatic assemblies. Department of Energy Conversion and Storage, Technical University of Denmark (2016)
24. M.A. Benedict, S.A. Sherif, D.G. Beers, M.G. Schroeder, Science and Technology for the Built Environment **22**(5), 520 (2016). DOI 10.1080/23744731.2016.1185889
25. P.V. Trevizoli, J.A. Lozano, G.F. Peixer, J.R. Barbosa, Jr., Journal of Magnetism and Magnetic Materials **395**, 109 (2015)
26. T. Lei, K. Engelbrecht, K.K. Nielsen, C.T. Veje, Applied Thermal Engineering **111**, 1232 (2017)
27. I. Niknia, O. Campbell, T.V. Christiaanse, P. Govindappa, R. Teyber, P.V. Trevizoli, A. Rowe, Applied Thermal Engineering **106**, 601 (2016). DOI 10.1016/j.applthermaleng.2016.06.039